

Electronic Supplementary Information

Metal-ligand delocalization of iron and cobalt porphyrin complexes in aqueous solutions probed by soft X-ray absorption spectroscopy

Masanari Nagasaka,^{*ab} Shota Tsuru,^{cd} Yasuyuki Yamada^{ef}

^a Institute for Molecular Science, Myodaiji, Okazaki 444-8585, Japan

^b Graduate Institute for Advanced Studies, SOKENDAI, Myodaiji, Okazaki 444-8585, Japan

^c Lehrstuhl für Theoretische Chemie, Ruhr-Universität Bochum, D-44780 Bochum, Germany

^d RIKEN Center for Computational Science, RIKEN, Kobe 650-0047, Japan

^e Department of Chemistry, Graduate School of Science, Nagoya University, Nagoya 464-8602, Japan

^f Research Center for Materials Science, Nagoya University, Nagoya 464-8602, Japan

* E-mail: nagasaka@ims.ac.jp

Table of Contents	Page
S1. Discussion on various methods for XAS of metal complexes	S2
S2. Application of dilute samples in the present XAS measurement system	S2
S3. Discussion of dimerization of metal complexes	S3
S4. Peak positions in metal L ₃ -edge XAS spectra of central metals	S4
S5. Peak positions in nitrogen K-edge XAS spectra of ligands	S5
S6. Effects of the approximations on computational inner-shell spectra	S7
S7. Change of 3d orbital energies with respect to spin multiplicity	S11
S8. Induced polarization effect for each spin state	S12
S9. Cartesian coordinates of all the calculated structures	S14
References	S27

S1. Discussion on various methods for XAS of metal complexes

Soft X-ray absorption spectroscopy (XAS) has an advantage in investigating metal-ligand delocalization of metal complexes with different central metals and the coordination of the solvent molecules to a metal complex in solutions by measuring the electronic structures of ligands at the nitrogen K-edge. Nevertheless, it is difficult to measure XAS spectra of metal complexes in solutions since soft X-rays are strongly absorbed by air and liquids.¹ For measuring XAS of metal complexes in solutions in transmission mode, it is necessary to prepare thin liquid layers with the thickness of several micrometers. Due to such severe measurement conditions, XAS spectra have been obtained by detecting fluorescent light that is emitted via the decay process following the core electron excitation with soft X-rays. XAS of metal complexes were measured in fluorescence yield by preparing microjets in vacuum conditions.²⁻⁴ Liquid cells including the 100 nm thick Si₃N₄ or SiC membranes were also used for XAS in fluorescence yield.^{2, 5-9} Note that XAS spectra in fluorescence yield deviate from true absorption spectra due to the self-absorption effect, where fluorescence light is absorbed by liquid samples itself. It should be noted that the low emission probability of fluorescence light can lead to the radiation damage of liquid samples.

The XAS measurement in transmission mode is effective for metal complexes because the radiation damage can be reduced by using soft X-rays with a low photon flux. The true spectrum can be simply obtained from the transmission measurement based on the Beer-Lambert law. Recently, XAS spectra of liquid samples have been extensively measured by generating flat microjets with the thickness of several micrometers.¹⁰⁻¹³ A major advantage of the flat-jet technique is absence of sample radiation damage due to the window-less system. However, the XAS measurements of flat microjets cannot be applied to liquid samples with high vapor pressure. Meanwhile, the XAS measurements of liquid samples have been performed by using liquid cells, where the liquid layer is sandwiched between two Si₃N₄ or SiC membranes.¹⁴ Because liquid samples are exchangeable by using syringe pumps, there is basically no limit to sample selection for the XAS measurements using liquid cells. The applications to the *operando* XAS observations of catalytic and electrochemical reactions in solutions are also possible by controlling the reaction conditions such as liquid temperature, pH, electrode potential, *etc.* Recently, we have realized the XAS measurements of liquid samples in transmission mode using liquid cells, where the liquid thickness is precisely controlled for obtaining appropriate absorbance of soft X-rays.^{15, 16} We have performed *operando* XAS observations of catalytic¹⁷ and electrochemical reactions in solutions.¹⁸ The photoexcitation dynamics of iron phenanthroline aqueous solutions have been investigated from the ligand side by using the N K-edge time-resolved XAS measurements based on liquid cells.¹⁹

S2. Application of dilute samples in the present XAS measurement system

For applying the XAS measurements to precious samples that are difficult to synthesize in large quantities, it is necessary to measure XAS of dilute solutions of metalloporphyrins. To evaluate the present XAS measurement system, we have measured the N K-edge XAS spectrum of 10 mM pyridine aqueous solutions, as shown in Fig. S1. Because we have developed precise thickness control method of liquid layers,^{15, 16, 20, 21}

the optical length of soft X-rays can increase for obtaining the appropriate absorbance of liquid samples. We have clearly observed C=N π^* peak of pyridine even in 10 mM aqueous solution. Considering the peak intensity and signal-to-noise ratio, it is possible to apply our developed system to several mM aqueous solution. It means that the N K-edge XAS of ligands in metalloporphyrins can be obtained even in dilute solution with several mM concentrations in aqueous solution.

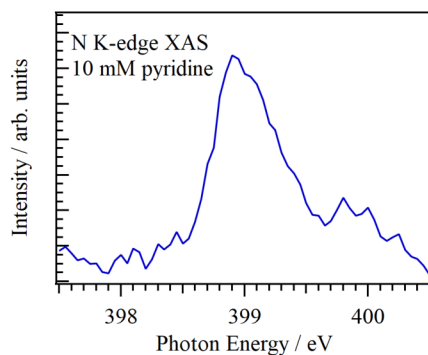


Figure S1. Nitrogen K-edge XAS spectrum of 10 mM pyridine aqueous solution measured by a transmission-type liquid cell.

As described above, the detection limit of C and N K-edge XAS is several mM in aqueous solution. In organic solvents, the detection limit of XAS depends on both the sorts of solute and solvent molecules. In the C K-edge XAS, the C=C π^* peaks (285 eV) and C=N π^* peaks (286 eV) of several mM solutes can be observed in the organic solvents which consist of single bonds such as methanol, ethanol, tetrahydrofuran, *etc.* because these peaks are below the first peak of methanol (288 eV).²² Thus, the C K-edge XAS of several mM metalloporphyrin can detect the C=N π^* peaks of ligands even in organic solvents, such as tetrahydrofuran. Meanwhile, because the energetic position of the C=O π^* peaks are around 290 eV, the C=O π^* peaks cannot be observed in organic solvents.

The detection limit of N K-edge XAS becomes higher and would be 100 mM in organic solvents. Soft X-rays at the N K-edge (400 eV) are also absorbed by organic solvents because the photon energy of the N K-edge is close to that of the C K-edge. In the soft X-ray beamline, monochromatic soft X-rays include not only first-order X-rays (400 eV) but also the high-order X-rays (800 eV, 1200 eV, *etc.*) due to the high order diffraction of a plane grating monochromator. Because of the absorption of the first-order X-rays (400 eV) by the organic solvents, the ratio of the high-order X-rays is increased compared to the first-order X-rays, resulting in the increase of the detection limit of the N K-edge XAS.

The L_{2,3}-edges of transition metals such as Mn, Fe, Co, *etc.* are above K-edges of C, N, and O. The detection limit of the central metal ions of metalloporphyrins is several mM in both aqueous solutions and organic solvents because the metal L_{2,3}-edges are not influenced by the K-edges of C, N, and O.

S3. Discussion of dimerization of metal complexes

The previous studies indicated that FePPIX form a cofacial dimer as shown in Fig. S2, where two

five-coordinated FePPIX are stacked, in this condition ($[\text{FePPIX}] = 50 - 100 \text{ mM}$ in 0.5 M aqueous NaOH).^{8, 23} Although Fe L_3 -edge X-ray emission spectra are influenced by the dimerization of FePPIX, Golnak *et al.* observed that Fe L_3 -edge XAS spectra of FePPIX dimers do not qualitatively differ from those of monomers.⁸ They also observed no large spectral difference between N K-edge XAS of FePPIX monomers and dimers.⁴

On the other hand, FePPIX and CoPPIX have the potential for forming μ -oxo-bridged dimer complexes under this condition. However, the intrinsic coordination geometries around the metal centers (M) of both forms (monomer and dimer) are identical as long as both complexes have the same coordination numbers ($(\text{HO})\text{MPPIX}$ and $\text{MPPIX}-\mu\text{O}-\text{MPPIX} / (\text{HO})\text{MPPIX}(\text{OH})$ and $(\text{HO})\text{MPPIX}-\mu\text{O}-\text{MPPIX}(\text{OH})$).

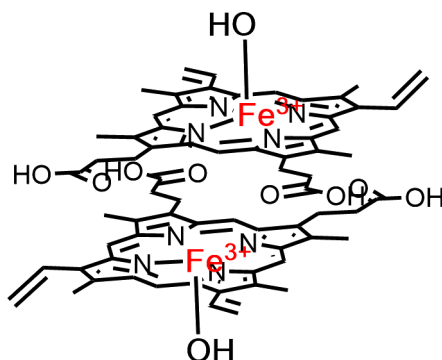


Figure S2. Molecular structures of hemin dimer.

S4. Peak positions in metal L_3 -edge XAS spectra of central metals

As shown in Fig. 2, the lowest peaks in metal L_3 -edge XAS spectra of metal porphyrin complexes in aqueous solutions consist of three peaks, where the lowest photon energy peaks are named first peaks, second lowest photon energy peaks are named second peaks, and the strong peaks in the third lowest photon energies are named main peaks. Table S1 shows the energetic positions of the first, second, and main peaks in both Fe L_3 -edge XAS spectrum of iron protoporphyrin IX (FePPIX) and Co L_3 -edge XAS spectrum of cobalt protoporphyrin IX (CoPPIX) in aqueous solutions obtained by fitting procedures. Table S1 also shows the energy shifts of the first and second peaks from the main peaks in the spectra of FePPIX and CoPPIX.

Table S1. Energetic positions of the first, second, and main peaks in Fe L_3 -edge XAS spectrum of FePPIX and Co L_3 -edge XAS spectrum of CoPPIX in aqueous solutions. The energy shifts of the first and second peaks from the main peaks ($\Delta E_{f,s-m}$) in the spectra of FePPIX and CoPPIX are also shown.

Metal L_3 -edge experiment		Energy / eV	$\Delta E_{f,s-m}$ / eV
FePPIX	First peak	707.046 ± 0.071	-2.395
	Second peak	708.118 ± 0.037	-1.323
	Main peak	709.441 ± 0.013	
CoPPIX	First peak	777.709 ± 0.050	-3.268
	Second peak	779.415 ± 0.055	-1.562
	Main peak	780.977 ± 0.041	

S5. Peak positions in nitrogen K-edge XAS spectra of ligands

Table S2 shows the experimentally obtained energetic positions of the first and second C=N π^* peaks in N K-edge XAS spectra of ligands in FePPIX, CoPPIX, and protoporphyrin IX (PPIX) in aqueous solutions, which are shown in Fig. 3. These peak positions were obtained from the fitting procedures with Gaussian profiles, where the full width at half maximum was 0.7 eV. Table S2 also shows the energy shifts of the first peaks in the spectra of CoPPIX and PPIX from the first peak in the spectrum of FePPIX as well as the energy shift of the second peak from the first peak in each spectrum.

Table S3 shows calculated energetic positions of the first and second C=N π^* peaks in N K-edge inner-shell spectra of FePPIX, CoPPIX, and PPIX, which are shown in Fig. 4. For comparison with the experiments, Table S3 also shows the energy shifts of the first peaks in the calculated spectra of CoPPIX and PPIX from the first peak in the spectrum of FePPIX as well as the energy shift of the second peak from the first peak in each calculated spectrum.

Table S4 shows the natural transition orbitals (NTOs)²⁴⁻²⁷ of the lowest eight excitations forming the first and second C=N π^* peaks in N K-edge inner-shell spectrum of PPIX.

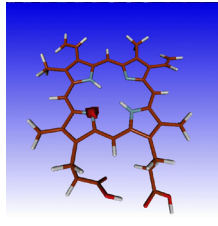
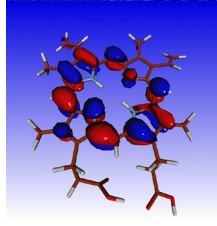
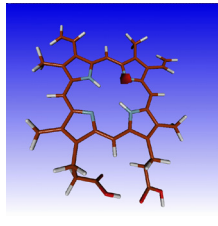
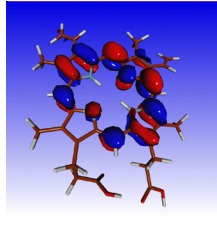
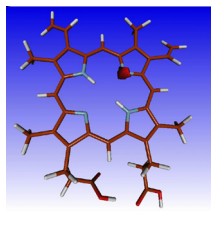
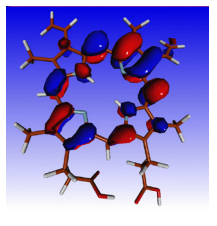
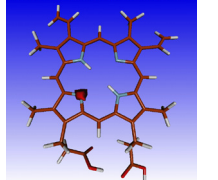
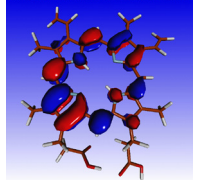
Table S2. Experimentally obtained energetic positions of the first and second C=N π^* peaks in N K-edge XAS spectra of FePPIX, CoPPIX, and PPIX in aqueous solutions. The energy shifts of the first peaks in the spectra of CoPPIX and PPIX from the first peak in the spectrum of FePPIX (ΔE) are shown. The energy shift of the second peak from the first peak (ΔE_{s-f}) in each spectrum is also shown.

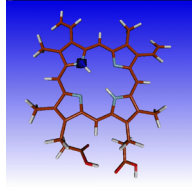
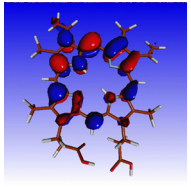
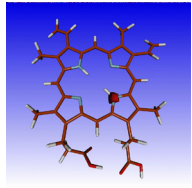
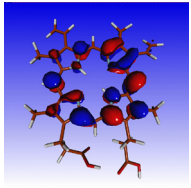
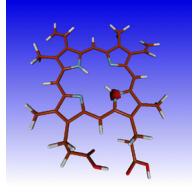
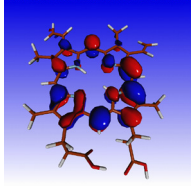
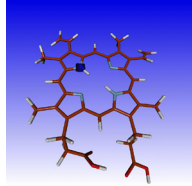
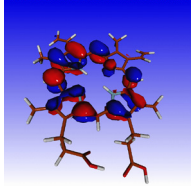
N K-edge XAS experiment		Energy / eV	ΔE / eV	ΔE_{s-f} / eV
FePPIX	First peak	398.592 ± 0.033		
	Second peak	399.302 ± 0.067		0.710
CoPPIX	First peak	398.731 ± 0.042	0.139	
	Second peak	399.559 ± 0.054		0.828
PPIX	First peak	397.760 ± 0.006	-0.832	
	Second peak	399.929 ± 0.006		2.169

Table S3. Calculated energetic positions of the first and second C=N π^* peaks in N K-edge inner-shell spectra of FePPIX, CoPPIX, and PPIX. The energy shifts of the first peaks in the calculated spectra of CoPPIX and PPIX from the first peak in the spectrum of FePPIX (ΔE) are shown. The energy shift of the second peak from the first peak (ΔE_{s-f}) in each calculated spectrum is also shown.

N K-edge inner-shell calculation		Energy / eV	ΔE / eV	ΔE_{s-f} / eV
FePPIX	First peak	397.75		
	Second peak	398.63		0.88
CoPPIX	First peak	398.19	0.44	
	Second peak	399.17		0.98
PPIX	First peak	397.76	0.01	
	Second peak	399.68		1.92

Table S4. Occupied and virtual orbitals between which electronic transition takes place in each excitation.

Energy / eV	Oscillator Strength	Occupied Orbital	Virtual Orbital
397.73	0.0175		
397.79	0.0177		
397.90	0.0005		
397.90	0.0007		

399.65	0.0117		
399.68	0.0088		
399.70	0.0051		
399.79	0.0022		

S6. Effects of the approximations on computational inner-shell spectra

The time-dependent density functional theory (TDDFT) calculations in the present work are based on the following approximations.

- (1) Tamm-Dancoff approximation (TDA).
- (2) Absence of correlation with the relevant core orbitals.
- (3) The def2-TZVPP basis set is perhaps not large enough to evaluate the overlap between the C=N π^* orbitals of the ligand and the 3d orbitals of the central metal ions.
- (4) Substitution of the counter anion (from Cl^- to OH^-) and the solvent effects are not considered.
- (5) Relativistic effects are not considered.

We conducted several test calculations for CoPPIX to account for how the approximations above influenced on the energetic positions and the intensities of the peaks.

Table S5 shows the positions and the total oscillator strength of the first and second C=N π^* peaks in N K-edge inner-shell spectrum of CoPPIX obtained by TDDFT calculations in conjunction with the CAM-B3LYP functional²⁸ under several different conditions. The first calculation is the one used for Fig. 4. In the second calculation, TDA is not applied, and the applied basis set is def2-TZVPP as the first calculation. In the third calculation, the applied basis set is changed from def2-TZVPP of the second calculation to cc-pCVTZ on the N atoms and cc-pVTZ on the others, to correlate the N 1s orbitals. In the fourth calculation, the applied basis set is changed from def2-TZVPP of the first calculation to cc-pVQZ on the Co and N atoms

and cc-pVTZ on the others, for more accurate overlap integral between the Co and N atoms. The results indicate that the approximations (1), (2), and (3) are irrelevant to the degree of agreement between the present experimental and computational inner-shell spectra.

Table S5. Calculated energetic positions of the first and second C=N π^* peaks in N K-edge inner-shell spectrum of CoPPIX as the average of each four equivalent core excitations as well as the total oscillator strength of each peak. The four calculations are distinguished from each other by whether the Tamm-Dancoff approximation (TDA) is applied and the adopted basis sets. The energy shift of the second peak from the first peak (ΔE_{s-f}) in each calculation is also shown. Excitation energies are not shifted, because the systematic error depends on the size of the basis set.

N K-edge inner-shell calculation for CoPPIX	Average N 1s excitation energy / eV	Total oscillator strength	ΔE_{s-f} / eV
TDA/def2-TZVPP	386.26	0.03342	0.97
	387.23	0.04185	
Full TDDFT/def2-TZVPP	386.26	0.03280	0.97
	387.23	0.04170	
Full TDDFT/cc-pCVTZ on N and cc-pVTZ on others	386.26	0.03245	0.98
	387.24	0.04160	
TDA/cc-pVQZ on Co and N, and cc-pVTZ on others	386.17	0.03265	0.98
	387.15	0.04167	

Figure S3 shows (a) the N K-edge inner-shell spectrum calculated for CoPPIX applying TDA and adopting the def2-TZVPP basis set (same as that of Fig. 4) and (b) that calculated for the CoPPIX complex where the Cl^- anion is substituted with the OH^- anion. The geometry for Fig. S3(b) was independently optimized at the DFT/PBE0/def2-TZVPP level. The energy difference between the first and second peaks in Fig. S3(a) is reasonably accurate compared to the experimental spectrum, which are described in Tables S2 and S3, despite poor reproduction of the intensities in Fig. 3. Meanwhile, the first peak in Fig. S3(b) shows a higher energy shift compared to that in Fig. S3(a), whereas the positions of the second peaks are almost equal. The two peaks are combined in the inner-shell spectrum of CoPPIX with the counter ion of OH^- .

As shown in Fig. 6, the positions of the first and second peaks in the N K-edge inner-shell spectrum of CoPPIX are related to the energetic positions of the d_{z^2} and $d_{x^2-y^2}$ orbitals of the Co^{3+} ion under the ligand-field effect, respectively. The substitution of the counter anion from Cl^- to OH^- barely shifts the energetic position of the $d_{x^2-y^2}$ orbital due to absence of the repulsive interaction, which explains the fixed position of the second peak. Meanwhile, the repulsive interaction affects the energetic position of the d_{z^2} orbital. Therefore, it is plausible that the repulsive interaction is underestimated in Fig. S3(a) by neglecting the substitution of the counter anion while it is overestimated in Fig. S3(b).

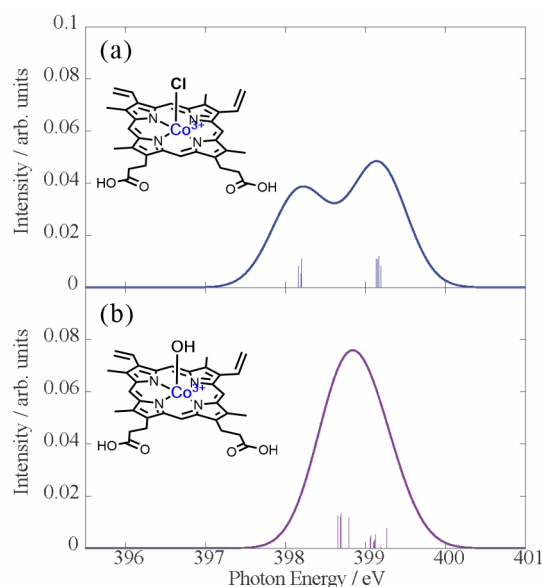


Figure S3. Calculated C=N π^* peaks in the N K-edge inner-shell spectra of CoPPIX where the counter anion is (a) Cl^- or (b) OH^- . Solvent effects other than the replacement of the anion are not considered.

The overestimation of the repulsive interaction with the OH^- anion might be due to the absence of the solvent effects in the present calculation. In the optimized geometry, the Co–O bond distance is 1.80 Å, which is close to the predicted Cu(III)–O bond distance of the $[\text{CuOH}]^{2+}$ core of some complexes.²⁹ Meanwhile, the bond distance between the Co^{3+} ion and the oxygen atom of the coordinated neutral water molecule is 2.07 Å in the optimized structure of octahedral CoPPIX complex used for Fig. 6. Since the coordinated OH^- anion of the CoPPIX complex is in the hydrogen bond network of the solvent, the Co–O bond distance of the solvated CoPPIX complex may fluctuate and be longer than 1.80 Å in average. As a result, the energetic position of the d_{z^2} orbital of Co^{3+} may not be as a higher energy shift as the simulation for Fig. S3(b) predicts. It should be also emphasized that the dipole-dipole interaction between the CoPPIX complex and the solvent water molecules might stabilize the final core excited states, which are polarized due to electron transfer from the N 1s orbitals of the ligand to the 3d orbitals of the Co^{3+} ion. This stabilization due to the dipole-dipole interaction can cause relatively large lower energy shift of the C=N π^* peaks in N K-edge inner-shell spectrum of CoPPIX (as well as FePPIX) in comparison with those in the spectrum of PPIX. These facts indicate that the approximation (4) is likely one cause of the mismatch between the measured and computed N K-edge inner-shell spectra.

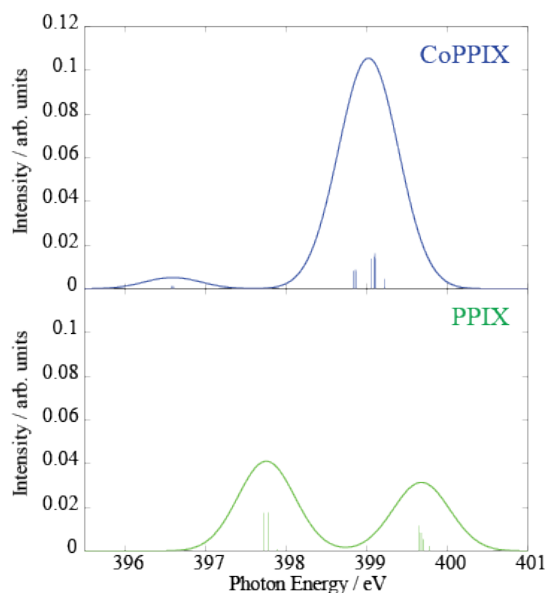


Figure S4. C=N π^* peaks in the N K-edge calculated inner-shell spectra of (upper) CoPPIX and (lower) PPIX considering the scalar relativistic effects with the second-order Douglas–Kroll method adopting the cc-pVTZ-DK basis set. Both the spectra are shifted by +11.66 eV to align the first peak in the experimental and computational spectra of PPIX.

To account for the relativistic effects in the N K-edge inner-shell spectra, we conducted inner-shell calculations applying TDA and adopting the cc-pVTZ-DK basis set for CoPPIX and PPIX, considering the scalar relativistic effects with the second-order Douglas–Kroll method,³⁰⁻³² as shown in Fig. S4. The scalar relativistic effects do not practically influence on the N K-edge inner-shell spectrum of PPIX. On the contrary, the N K-edge inner-shell spectrum of CoPPIX shown in Fig. S4 is totally different from that shown in Fig. 4, although the agreement with the experimental spectrum is poorer when the scalar relativistic effects are considered.

The scalar relativistic effects appearing in the N K-edge inner-shell spectrum of CoPPIX might be explained by the atomic spinor and orbital energies, which were summarized by Tatewaki *et al.* (Table S1 of this reference).³³ Considering those of the atomic number $Z = 10$, the shifts of the C=N π^* orbitals of the ligand are estimated as less than 0.1 eV. Meanwhile, those of the atomic number $Z = 28$ indicate that the 3d orbitals of Co^{3+} experience a higher energy shift by more than 0.5 eV. As clearly shown in Fig. 5(a), the larger energy shift of the 3d orbitals of Co^{3+} than that of the C=N π^* orbitals of the ligand results in the energy shift of the virtual orbitals of the complex. It causes the energy shifts of the C=N π^* peaks in the N K-edge inner-shell spectra of CoPPIX, as shown in Fig. 6. Therefore, the approximation (5) is also likely one cause of the mismatch between the measured and computed N K-edge inner-shell spectra.

In conclusion, both the solvent and relativistic effects need to be considered for more quantitative simulation of the inner-shell spectra of the PPIX complexes. In fact, difficulty in the inner-shell calculations for the PPIX complexes is not limited to these two aspects: The reference ansatz is prone to the instability for

systems with partially filled d orbitals. Moreover, no functional always reproduces core binding energies of metal atoms and complexes with partially filled d orbitals.³⁴ Nevertheless, the present non-relativistic calculations neglecting the solvent effects and the substitution of the counter anion have given reasonably accurate results probably due to cancellation of errors. The present results may indicate that information on the electron configuration and the spin multiplicity as well as the coordination number of complexes reflected in the inner-shell spectra of the ligand can be extracted with simple TDDFT calculations.

S7. Change of 3d orbital energies with respect to spin multiplicity

Figure S5 schematically shows the SCF and 3d orbital energies calculated for (upper) the spin doublet and sextet states of FePPIX and (lower) the spin singlet and triplet states of CoPPIX. The calculations were conducted with the restricted (open-shell) DFT [R(O)DFT] scheme adopting the CAM-B3LYP functional and the def2-TZVPP basis set at the geometries optimized at the DFT/PBE0/def2-TZVPP level. The diagrams of the spin quadruplet state of FePPIX and the spin quintuplet state of CoPPIX are guesses with interpolation and extrapolation, respectively, because RODFT does not give stable results for these configurations. The obtained orbital energies are relative ones with respect to the degenerate d_{zx} and d_{yz} orbitals.

Comparing the results obtained for the spin doublet and sextet states of FePPIX, the reduced screening effect and the increased exchange interaction in the spin sextet state bring about relaxation of the 3d orbitals, which even exceeds the energy to raise two electrons. Meanwhile in case of the spin singlet and triplet states of CoPPIX, such effects are insufficient to raise one electron and the spin triplet state energetically lies higher than the spin singlet state.

These R(O)DFT results numerically support the interpretation shown in Fig. 5(b) of the experimentally confirmed result that the highest and lowest spin multiplicity is the most stable for FePPIX and CoPPIX, respectively, as follows. The high spin (spin sextet) state of FePPIX complex is stabilized by only $0.0126 E_h$ (0.34 eV , 2765 cm^{-1}) than the low spin (spin doublet) state. Meanwhile, the energy required to raise each electron from the d_{zx} and d_{yz} orbitals to the d_{z^2} and $d_{x^2-y^2}$ orbitals is estimated as 3.72 eV ($0.1367 E_h$, 30004 cm^{-1}). Therefore, the pairing energy is about 2.0 eV in the case of FePPIX complex. Since the estimated pairing energy is sufficiently larger than the stabilization by the parallel spin configuration, the formation of at least one electron pair in the CoPPIX complex is the factor dominating the spin multiplicity.

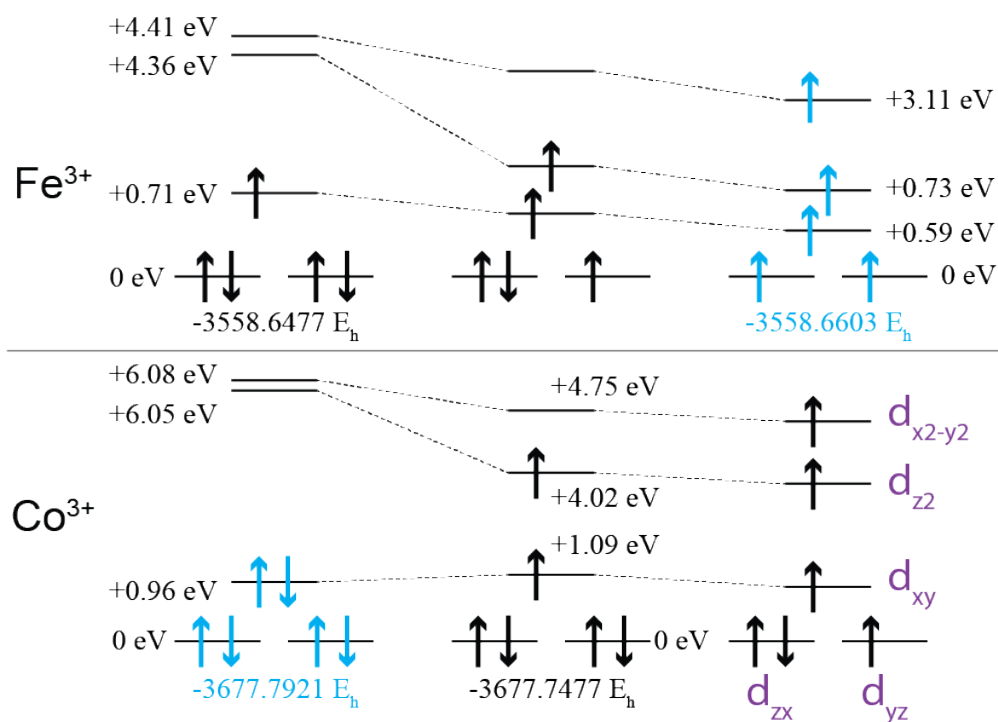


Figure S5. SCF and 3d orbital energies calculated for (upper) FePPIX and (lower) CoPPIX with R(O)DFT. The orbital energies are shown with respect to those of the degenerate d_{zx} and d_{yz} orbitals for each configuration. Arrows indicating the electrons and the SCF energies are sky-blue colored for the high-spin (spin sextet) state of FePPIX and the low-spin (spin singlet) state of CoPPIX to emphasize that these spin multiplicities are the experimentally confirmed ones.

S8. Induced polarization effect for each spin state

Figure S6 schematically shows the 3d orbital energies of the spin doublet and sextet states of FePPIX and the monovalent cation of CoPPIX, obtained by RODFT in conjunction with the CAM-B3LYP functional adopting the def2-TZVPP basis set. The monovalent cation of CoPPIX mimics core-ionized states of FePPIX and qualitatively exhibit the induced polarization effect on the orbitals after the core excitations, in the manner of the equivalent core or ($Z + 1$) approximation.³⁵ Comparison of the d_{z₂} and d_{x₂-y₂} orbital energies with respect to that of the N 1s orbital enables us to estimate how the positions of the first and second peaks in the N K-edge XAS spectrum of FePPIX change with respect to the spin multiplicity, because these core excitations are dominated by transitions from the N 1s orbital to the d_{z₂} and d_{x₂-y₂} orbitals. We also conducted RDFT calculation for the monovalent cation of nickel protoporphyrin IX (NiPPIX), which mimics core-ionized state of CoPPIX, to estimate relationship between the peak positions and the atomic number of the transition metal ion in the cases of N 1s excitations from the low-spin states.

For the high-spin (spin sextet) state of the CoPPIX cation, the d_{z₂} and d_{x₂-y₂} orbitals lie in lower energetic positions with respect to the N 1s orbitals in comparison with those for the low-spin (spin doublet) state. Moreover, the separation between the d_{z₂} and d_{x₂-y₂} orbitals are smaller for the high-spin state than for

the low-spin state. In addition to the estimation for the different spin multiplicity of FePPIX, the estimation for the low-spin state of CoPPIX using the monovalent cation of NiPPIX predicts that the first peak in the N K-edge inner-shell spectrum of FePPIX would lie in higher energetic position than that in the inner-shell spectrum of CoPPIX if the FePPIX complex were in the low-spin (spin doublet) state. This prediction is in accord with the tendency that the atomic radius is smaller when the atomic number is bigger within elements in a certain same period, due to incomplete screening effect by electrons in outer orbitals to the nuclei. Although this approximation might overestimate the induced polarization effect by considering relaxation of the core orbitals of the central metal, which does not occur in the N 1s excitations, this result supports the interpretation relating the lower energy shift and the smaller distance of the first and second peaks in the N K-edge XAS spectrum of FePPIX compared to those of CoPPIX with the higher spin multiplicity of FePPIX.

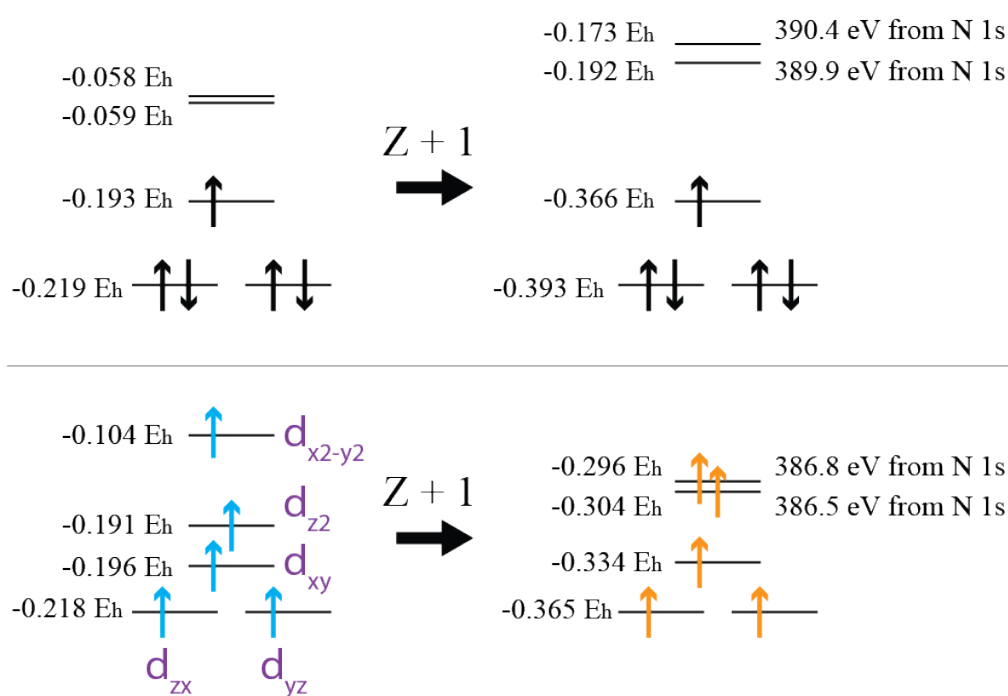


Figure S6. 3d orbital energies calculated for (upper) the low-spin state and (lower) the high-spin state of (left) FePPIX and (right) the monovalent cation of CoPPIX with RODFT. The monovalent cation of CoPPIX mimics core-ionized states of FePPIX. Arrows indicating the electrons are sky-blue and orange colored for the high-spin state of FePPIX and the CoPPIX cation, respectively, to emphasize that this spin multiplicity (sextet) is the experimentally confirmed one. In case of the monovalent cation of NiPPIX mimicking core-ionized states of CoPPIX in the low-spin state, the orbitals energies of d_{z^2} and $d_{x^2-y^2}$ are 389.1 eV and 390.8 eV with respect to the N 1s orbitals, respectively.

S9. Cartesian coordinates of all the calculated structures

(xyz format with the Å unit)

76

Protoporphyrin IX (PPIX)

N	-2.3880245	1.6116792	0.1149782
C	-2.0107985	2.9041817	0.1614474
C	-3.7333216	1.6296120	-0.0362176
C	-3.1582326	3.8025931	0.0281414
C	-4.2491049	2.9892644	-0.0889604
C	-3.0830041	5.2492590	0.0659755
H	-2.2295681	5.6639550	0.5964589
C	-3.9443267	6.1145198	-0.4731322
H	-3.7941439	7.1811899	-0.3649973
H	-4.8003724	5.7972157	-1.0538573
C	-5.6790387	3.3751136	-0.2021857
H	-6.3381490	2.6166988	0.2225335
H	-5.8651731	4.3147013	0.3222800
H	-5.9816778	3.5219693	-1.2438434
C	-0.6968139	3.3495423	0.2950354
H	-0.5344018	4.4193403	0.2845326
N	0.4798473	1.2169203	0.4644644
H	-0.3321200	0.6169811	0.4177867
C	0.4424965	2.5749645	0.4218785
C	1.7565790	0.7743495	0.6011762
C	1.7958035	3.0396489	0.5257653
C	2.6016762	1.9337542	0.6340983
C	2.1968808	4.4715918	0.4964134
H	1.6603404	5.0513485	1.2509101
H	3.2634177	4.5912207	0.6856067
H	1.9815552	4.9273491	-0.4736434
C	4.0894843	1.8911373	0.6942302
H	4.4687191	2.7998339	1.1679314
H	4.4215048	1.0559683	1.3150056
C	4.7132907	1.7481886	-0.7065408
H	4.4564649	2.6060401	-1.3259607
H	4.3386403	0.8412864	-1.1877381
C	6.1985328	1.6115656	-0.6095445

O	6.7788902	0.6475174	-0.1606871
O	6.8657455	2.6829318	-1.0388729
H	7.8074749	2.4975396	-0.9249726
C	2.1463884	-0.5519043	0.6822034
H	3.2029628	-0.7247340	0.8393344
N	-0.0018915	-1.6471070	0.3706993
C	1.3340335	-1.6765910	0.5624111
C	-0.3834338	-2.9414206	0.2894871
C	1.8396719	-3.0478890	0.6117785
C	0.7541843	-3.8429777	0.4311214
C	3.2503416	-3.4853620	0.8319839
H	3.2312734	-4.5038382	1.2242268
H	3.7292367	-2.8791785	1.6041419
C	4.1448981	-3.4820146	-0.4226082
H	4.9592326	-4.1956117	-0.2674272
H	3.5864633	-3.7896911	-1.3045353
C	4.8000961	-2.1619850	-0.7249400
O	4.7109524	-1.5697613	-1.7716365
O	5.5218143	-1.7212203	0.3072111
H	5.9680777	-0.8760271	0.0677743
C	0.6812230	-5.3273071	0.3809894
H	-0.0365570	-5.7202701	1.1057661
H	1.6477218	-5.7830262	0.5961766
H	0.3680177	-5.6795196	-0.6058052
C	-1.6857052	-3.3919862	0.1081879
H	-1.8235135	-4.4643233	0.0612482
N	-2.8818179	-1.2685625	0.0053625
H	-2.0715602	-0.6692856	0.0839727
C	-4.1576039	-0.8256143	-0.1224734
C	-2.8372245	-2.6283749	-0.0163438
C	-4.9987547	-1.9869786	-0.2430457
C	-4.1779848	-3.0979469	-0.1732306
C	-6.4406170	-1.9145760	-0.3700524
H	-6.8903955	-0.9823681	-0.0406459
C	-7.2616769	-2.8550687	-0.8402447
H	-8.3294026	-2.6808930	-0.8735366
H	-6.9096139	-3.8024517	-1.2243629

C	-4.5771509	-4.5281782	-0.2043060
H	-3.8181052	-5.1668930	0.2464945
H	-5.5116645	-4.6782867	0.3403498
H	-4.7388517	-4.8825216	-1.2267002
C	-4.5456395	0.5041402	-0.1444704
H	-5.6038839	0.6830628	-0.2761722

76

Iron protoporphyrin IX (FePPIX)

Fe	-1.2529129	-0.0278899	0.8384749
Cl	-1.5182112	-0.0561507	3.0264102
N	-2.3859519	1.6103119	0.2238387
C	-1.9929308	2.9112506	0.2419232
C	-3.7383336	1.6201865	0.0423418
C	-3.1308627	3.7853021	0.0651552
C	-4.2275297	2.9690668	-0.0521546
C	-3.0536612	5.2338360	0.0592564
H	-2.2293704	5.6653624	0.6207827
C	-3.8851400	6.0736457	-0.5583924
H	-3.7443028	7.1443045	-0.4830328
H	-4.7081840	5.7296330	-1.1710915
C	-5.6527236	3.3575476	-0.2065247
H	-6.3199499	2.6294320	0.2561183
H	-5.8360533	4.3272453	0.2593309
H	-5.9408911	3.4427869	-1.2587027
C	-0.6819553	3.3388386	0.3645400
H	-0.5074548	4.4058322	0.3351282
N	0.4194654	1.1702842	0.5412760
C	0.4339511	2.5315758	0.4828466
C	1.7182246	0.7761273	0.6480640
C	1.7870754	3.0232600	0.5397130
C	2.5899057	1.9254583	0.6390805
C	2.1760838	4.4570557	0.4778921
H	1.6957417	5.0346229	1.2714783
H	3.2533349	4.5833175	0.5854274
H	1.8849088	4.9108534	-0.4731102
C	4.0783958	1.8772381	0.6454793

H	4.4763422	2.7910542	1.0933486
H	4.4347555	1.0495207	1.2628332
C	4.6454046	1.7204163	-0.7783000
H	4.3549438	2.5701823	-1.3942870
H	4.2586766	0.8062326	-1.2346025
C	6.1344523	1.6011058	-0.7400862
O	6.7429772	0.6335209	-0.3378395
O	6.7718722	2.6925146	-1.1628999
H	7.7195321	2.5197286	-1.0836029
C	2.1477399	-0.5364970	0.7411832
H	3.2089731	-0.6976334	0.8747901
N	0.0007622	-1.6463845	0.4755795
C	1.3520657	-1.6645046	0.6444747
C	-0.3894193	-2.9478263	0.3742863
C	1.8397975	-3.0239933	0.6639613
C	0.7489644	-3.8239810	0.4846419
C	3.2533560	-3.4653502	0.8542208
H	3.2371912	-4.4738992	1.2708356
H	3.7552701	-2.8438764	1.5985203
C	4.1084329	-3.4945948	-0.4257626
H	4.9314718	-4.1988062	-0.2747060
H	3.5264251	-3.8301708	-1.2820728
C	4.7436268	-2.1775026	-0.7824610
O	4.6080143	-1.6104087	-1.8378240
O	5.4997713	-1.7111650	0.2116193
H	5.9381938	-0.8706641	-0.0612558
C	0.6849457	-5.3075040	0.4089248
H	-0.0241247	-5.7146976	1.1336760
H	1.6562049	-5.7595349	0.6076484
H	0.3650695	-5.6430290	-0.5812083
C	-1.6884651	-3.3796201	0.1860922
H	-1.8379422	-4.4486171	0.1142053
N	-2.8103012	-1.2175232	0.1298247
C	-4.1001034	-0.8229319	-0.0451447
C	-2.8124919	-2.5796152	0.0602696
C	-4.9558018	-1.9714898	-0.2429619
C	-4.1424168	-3.0742430	-0.1709704

C	-6.3911545	-1.8963433	-0.4387100
H	-6.8838795	-1.0331922	0.0006198
C	-7.1523405	-2.7722089	-1.0955274
H	-8.2225631	-2.6268923	-1.1684010
H	-6.7399913	-3.6378887	-1.5970977
C	-4.5235137	-4.5068253	-0.2636715
H	-3.8664480	-5.1371637	0.3365312
H	-5.5460834	-4.6529261	0.0882728
H	-4.4793260	-4.8753668	-1.2931097
C	-4.5310419	0.4912063	-0.0713561
H	-5.5870150	0.6548048	-0.2352839

76

Cobalt protoporphyrin IX (CoPPIX, five-coordinate)

Co	-1.2054960	-0.0207802	0.3357892
Cl	-1.4137440	-0.0441883	2.4736584
N	-2.3549963	1.5638480	0.0861799
C	-1.9788360	2.8726595	0.0673602
C	-3.7215801	1.5913316	0.0802387
C	-3.1247867	3.7486360	0.0140905
C	-4.2234478	2.9357285	0.0438957
C	-3.0471791	5.1971026	-0.0147934
H	-2.1733261	5.6370831	0.4579036
C	-3.9385636	6.0271337	-0.5570022
H	-3.7966048	7.0991358	-0.5075671
H	-4.8160352	5.6719848	-1.0816406
C	-5.6587650	3.3164288	0.0733420
H	-6.2491391	2.6124631	0.6614045
H	-5.7785032	4.3072202	0.5138564
H	-6.0943829	3.3505871	-0.9298353
C	-0.6788674	3.3167678	0.1009301
H	-0.5041517	4.3819326	0.0496411
N	0.3815596	1.1373248	0.3208830
C	0.4158750	2.4996566	0.2346841
C	1.6753786	0.7666325	0.5453563
C	1.7595205	2.9981395	0.3511828
C	2.5491060	1.9110449	0.5567765

C	2.1475005	4.4304514	0.2605682
H	1.6431532	5.0308843	1.0218315
H	3.2208331	4.5594916	0.3992450
H	1.8879609	4.8566769	-0.7119414
C	4.0321691	1.8657292	0.6878695
H	4.3868583	2.7877931	1.1552055
H	4.3371827	1.0499315	1.3465410
C	4.7221531	1.6922879	-0.6785426
H	4.4814368	2.5305651	-1.3303111
H	4.3839174	0.7682108	-1.1531796
C	6.2028783	1.5866602	-0.5077724
O	6.7808903	0.6318135	-0.0355324
O	6.8675669	2.6757770	-0.8925683
H	7.8056639	2.5123913	-0.7268383
C	2.1079851	-0.5266088	0.7153737
H	3.1528196	-0.6865912	0.9410620
N	-0.0261252	-1.5943750	0.2816440
C	1.3082721	-1.6333087	0.5651852
C	-0.3947147	-2.9027317	0.1563237
C	1.7959072	-2.9892968	0.6156956
C	0.7283517	-3.7828925	0.3338308
C	3.1886864	-3.4304685	0.9235700
H	3.1334664	-4.4329877	1.3515453
H	3.6328151	-2.8019555	1.6978207
C	4.1427778	-3.4824089	-0.2834239
H	4.9466783	-4.1885607	-0.0577291
H	3.6284338	-3.8269086	-1.1785529
C	4.8119579	-2.1735283	-0.6050439
O	4.7596824	-1.6167856	-1.6735950
O	5.4934659	-1.7011438	0.4385260
H	5.9564513	-0.8651621	0.1926614
C	0.6643374	-5.2650479	0.2375085
H	-0.0516985	-5.6833176	0.9493959
H	1.6343485	-5.7172357	0.4418329
H	0.3568376	-5.5888240	-0.7602380
C	-1.6726332	-3.3519002	-0.0608283
H	-1.8181258	-4.4187083	-0.1546463

N	-2.7651360	-1.1819314	-0.0025378
C	-4.0766336	-0.8121348	-0.0132867
C	-2.7839936	-2.5440337	-0.1124012
C	-4.9439028	-1.9557005	-0.1649312
C	-4.1230959	-3.0466116	-0.2355262
C	-6.3928648	-1.8852629	-0.1928268
H	-6.8397166	-1.0667579	0.3651423
C	-7.2147387	-2.7229997	-0.8252814
H	-8.2879219	-2.5949626	-0.7647724
H	-6.8517329	-3.5396244	-1.4359458
C	-4.4962578	-4.4795800	-0.3505463
H	-3.7979650	-5.1229579	0.1860840
H	-5.4924451	-4.6463859	0.0617718
H	-4.5146068	-4.8149465	-1.3919084
C	-4.5313731	0.4818125	0.0515192
H	-5.5993137	0.6420396	0.0253852

75

Planar CoPPIX without counter anion

Co	-1.2054960	-0.0207802	0.3357892
N	-2.3549963	1.5638480	0.0861799
C	-1.9788360	2.8726595	0.0673602
C	-3.7215801	1.5913316	0.0802387
C	-3.1247867	3.7486360	0.0140905
C	-4.2234478	2.9357285	0.0438957
C	-3.0471791	5.1971026	-0.0147934
H	-2.1733261	5.6370831	0.4579036
C	-3.9385636	6.0271337	-0.5570022
H	-3.7966048	7.0991358	-0.5075671
H	-4.8160352	5.6719848	-1.0816406
C	-5.6587650	3.3164288	0.0733420
H	-6.2491391	2.6124631	0.6614045
H	-5.7785032	4.3072202	0.5138564
H	-6.0943829	3.3505871	-0.9298353
C	-0.6788674	3.3167678	0.1009301
H	-0.5041517	4.3819326	0.0496411
N	0.3815596	1.1373248	0.3208830

C	0.4158750	2.4996566	0.2346841
C	1.6753786	0.7666325	0.5453563
C	1.7595205	2.9981395	0.3511828
C	2.5491060	1.9110449	0.5567765
C	2.1475005	4.4304514	0.2605682
H	1.6431532	5.0308843	1.0218315
H	3.2208331	4.5594916	0.3992450
H	1.8879609	4.8566769	-0.7119414
C	4.0321691	1.8657292	0.6878695
H	4.3868583	2.7877931	1.1552055
H	4.3371827	1.0499315	1.3465410
C	4.7221531	1.6922879	-0.6785426
H	4.4814368	2.5305651	-1.3303111
H	4.3839174	0.7682108	-1.1531796
C	6.2028783	1.5866602	-0.5077724
O	6.7808903	0.6318135	-0.0355324
O	6.8675669	2.6757770	-0.8925683
H	7.8056639	2.5123913	-0.7268383
C	2.1079851	-0.5266088	0.7153737
H	3.1528196	-0.6865912	0.9410620
N	-0.0261252	-1.5943750	0.2816440
C	1.3082721	-1.6333087	0.5651852
C	-0.3947147	-2.9027317	0.1563237
C	1.7959072	-2.9892968	0.6156956
C	0.7283517	-3.7828925	0.3338308
C	3.1886864	-3.4304685	0.9235700
H	3.1334664	-4.4329877	1.3515453
H	3.6328151	-2.8019555	1.6978207
C	4.1427778	-3.4824089	-0.2834239
H	4.9466783	-4.1885607	-0.0577291
H	3.6284338	-3.8269086	-1.1785529
C	4.8119579	-2.1735283	-0.6050439
O	4.7596824	-1.6167856	-1.6735950
O	5.4934659	-1.7011438	0.4385260
H	5.9564513	-0.8651621	0.1926614
C	0.6643374	-5.2650479	0.2375085
H	-0.0516985	-5.6833176	0.9493959

H	1.6343485	-5.7172357	0.4418329
H	0.3568376	-5.5888240	-0.7602380
C	-1.6726332	-3.3519002	-0.0608283
H	-1.8181258	-4.4187083	-0.1546463
N	-2.7651360	-1.1819314	-0.0025378
C	-4.0766336	-0.8121348	-0.0132867
C	-2.7839936	-2.5440337	-0.1124012
C	-4.9439028	-1.9557005	-0.1649312
C	-4.1230959	-3.0466116	-0.2355262
C	-6.3928648	-1.8852629	-0.1928268
H	-6.8397166	-1.0667579	0.3651423
C	-7.2147387	-2.7229997	-0.8252814
H	-8.2879219	-2.5949626	-0.7647724
H	-6.8517329	-3.5396244	-1.4359458
C	-4.4962578	-4.4795800	-0.3505463
H	-3.7979650	-5.1229579	0.1860840
H	-5.4924451	-4.6463859	0.0617718
H	-4.5146068	-4.8149465	-1.3919084
C	-4.5313731	0.4818125	0.0515192
H	-5.5993137	0.6420396	0.0253852

79

Octahedral CoPPIX with a hydrated water molecule

Co	-1.1827300	-0.0222684	0.2047510
Cl	-1.4223912	-0.0378289	2.3672281
N	-2.3544186	1.5832780	0.0162537
O	-0.9973405	0.0001820	-1.8580995
H	-1.6221549	-0.6863375	-2.1170436
H	-1.4280396	0.8337218	-2.0792617
C	-1.9781736	2.8889600	0.0802413
C	-3.7187878	1.5987759	-0.0470116
C	-3.1271079	3.7613129	0.0233162
C	-4.2228976	2.9438552	-0.0437912
C	-3.0571546	5.2092047	0.0828173
H	-2.2033062	5.6216656	0.6133099
C	-3.9317601	6.0686134	-0.4411506
H	-3.7965070	7.1359222	-0.3213669

H	-4.7886053	5.7445340	-1.0174754
C	-5.6591905	3.3233885	-0.0545627
H	-6.2748234	2.5811137	0.4548400
H	-5.8013926	4.2812256	0.4482621
H	-6.0491372	3.4291523	-1.0716235
C	-0.6776185	3.3315445	0.1788120
H	-0.5056976	4.3983947	0.1860401
N	0.4001060	1.1523732	0.3159053
C	0.4212974	2.5121599	0.2931587
C	1.6894901	0.7691842	0.5039876
C	1.7671450	3.0105375	0.4304299
C	2.5621753	1.9169504	0.5635166
C	2.1473783	4.4478703	0.4211856
H	1.6410577	5.0002973	1.2166412
H	3.2202984	4.5749403	0.5649436
H	1.8838398	4.9285340	-0.5245777
C	4.0466498	1.8647516	0.6713895
H	4.4140314	2.7826707	1.1365998
H	4.3587745	1.0434227	1.3202280
C	4.7113373	1.6940208	-0.7083062
H	4.4573705	2.5345717	-1.3521448
H	4.3628417	0.7718372	-1.1787552
C	6.1950633	1.5898988	-0.5661255
O	6.7860972	0.6265386	-0.1289375
O	6.8482439	2.6925717	-0.9332804
H	7.7893556	2.5300598	-0.7849789
C	2.1268362	-0.5293892	0.6308589
H	3.1764670	-0.6894401	0.8323588
N	-0.0124822	-1.6153973	0.2675441
C	1.3241869	-1.6402120	0.5112986
C	-0.3952126	-2.9192426	0.2077844
C	1.8106013	-2.9981676	0.6019461
C	0.7313667	-3.7982716	0.3956700
C	3.2113545	-3.4307936	0.8844106
H	3.1701090	-4.4290014	1.3234516
H	3.6688771	-2.7923037	1.6426582
C	4.1406871	-3.4899502	-0.3418623

H	4.9440496	-4.2018299	-0.1323226
H	3.6061509	-3.8315102	-1.2262153
C	4.8145086	-2.1873444	-0.6795414
O	4.7575157	-1.6390740	-1.7521559
O	5.5080092	-1.7108272	0.3543755
H	5.9691173	-0.8767648	0.0996286
C	0.6563316	-5.2830681	0.3766479
H	-0.0449011	-5.6591728	1.1257815
H	1.6280791	-5.7316688	0.5805358
H	0.3228027	-5.6554973	-0.5955076
C	-1.6804724	-3.3728339	0.0275459
H	-1.8302052	-4.4427300	-0.0041599
N	-2.7727637	-1.2017496	-0.0599936
C	-4.0767301	-0.8174776	-0.1273572
C	-2.7928683	-2.5665084	-0.0780985
C	-4.9478387	-1.9654499	-0.2265391
C	-4.1342371	-3.0656574	-0.1934523
C	-6.3950741	-1.8907460	-0.2974374
H	-6.8496484	-1.0237678	0.1740878
C	-7.2083923	-2.7763658	-0.8738847
H	-8.2815501	-2.6361749	-0.8522361
H	-6.8380685	-3.6475590	-1.3984840
C	-4.5190126	-4.5005586	-0.2051101
H	-3.8269820	-5.1074315	0.3797305
H	-5.5178042	-4.6290415	0.2150791
H	-4.5381051	-4.9124491	-1.2187594
C	-4.5238604	0.4841812	-0.1222409
H	-5.5896972	0.6461688	-0.1910691

77

CoPPIX where Cl⁻ is substituted to OH⁻

Co	-1.2125066	-0.0295775	0.3359027
O	-1.4221011	-0.0792678	2.1229214
H	-0.7527299	0.5115946	2.4773339
N	-2.3640725	1.5631035	0.0909441
C	-1.9876523	2.8706189	0.0716996
C	-3.7285776	1.5867030	0.0716583

C	-3.1344558	3.7464312	0.0022196
C	-4.2322169	2.9316589	0.0234352
C	-3.0582208	5.1945909	-0.0321203
H	-2.1831118	5.6367383	0.4364130
C	-3.9495394	6.0240946	-0.5758152
H	-3.8053881	7.0959960	-0.5303829
H	-4.8283533	5.6690345	-1.0981073
C	-5.6678683	3.3120351	0.0352077
H	-6.2671881	2.6034505	0.6083870
H	-5.7947713	4.2995685	0.4814439
H	-6.0886705	3.3542801	-0.9740417
C	-0.6869976	3.3144006	0.1269430
H	-0.5101411	4.3791656	0.0733081
N	0.3719251	1.1331920	0.3700606
C	0.4071485	2.4967321	0.2780001
C	1.6677268	0.7574849	0.5826870
C	1.7511441	2.9913466	0.3974272
C	2.5404912	1.9016253	0.5983861
C	2.1435403	4.4228502	0.3071054
H	1.6283180	5.0281000	1.0571047
H	3.2149053	4.5507365	0.4618301
H	1.8999775	4.8452986	-0.6712170
C	4.0242050	1.8551427	0.7215117
H	4.3821860	2.7728323	1.1950818
H	4.3332055	1.0328063	1.3701114
C	4.7055235	1.6942347	-0.6505941
H	4.4598742	2.5375878	-1.2939252
H	4.3642954	0.7738806	-1.1305114
C	6.1873884	1.5874321	-0.4914043
O	6.7680082	0.6339538	-0.0196134
O	6.8506060	2.6736405	-0.8871873
H	7.7898903	2.5085880	-0.7300392
C	2.1015482	-0.5398345	0.7312747
H	3.1476894	-0.7014264	0.9500330
N	-0.0299705	-1.6082641	0.2850764
C	1.3035483	-1.6468361	0.5648480
C	-0.4009004	-2.9133285	0.1557177

C	1.7924397	-3.0041641	0.6059943
C	0.7234551	-3.7959882	0.3256308
C	3.1863704	-3.4468200	0.9061535
H	3.1344445	-4.4544083	1.3225638
H	3.6315930	-2.8262122	1.6862640
C	4.1383378	-3.4830288	-0.3031826
H	4.9433796	-4.1912977	-0.0880140
H	3.6223469	-3.8168220	-1.2013852
C	4.8060868	-2.1702082	-0.6104138
O	4.7562356	-1.6033006	-1.6737063
O	5.4850863	-1.7065366	0.4391142
H	5.9469400	-0.8679273	0.2009769
C	0.6580443	-5.2777501	0.2249723
H	-0.0606801	-5.6970794	0.9335075
H	1.6267531	-5.7323478	0.4305034
H	0.3523883	-5.5982391	-0.7744315
C	-1.6815651	-3.3619115	-0.0551745
H	-1.8271581	-4.4286278	-0.1509980
N	-2.7769531	-1.1942828	0.0092922
C	-4.0850939	-0.8209509	-0.0090671
C	-2.7945507	-2.5542411	-0.1018635
C	-4.9548405	-1.9651060	-0.1598620
C	-4.1352223	-3.0569959	-0.2257746
C	-6.4034811	-1.8930512	-0.1910440
H	-6.8495164	-1.0665477	0.3557444
C	-7.2272980	-2.7365961	-0.8136056
H	-8.3001457	-2.6044316	-0.7555925
H	-6.8665862	-3.5619860	-1.4136622
C	-4.5098509	-4.4898270	-0.3379477
H	-3.8077580	-5.1333606	0.1935090
H	-5.5032870	-4.6564806	0.0813584
H	-4.5359157	-4.8252640	-1.3791719
C	-4.5381208	0.4751949	0.0456292
H	-5.6058554	0.6357638	0.0105341

References

- 1 C. T. Chantler, *J. Phys. Chem. Ref. Data*, 2000, **29**, 597-1048.
- 2 E. F. Aziz, S. Eisebitt, F. de Groot, J. W. Chiou, C. Dong, J. Guo and W. Eberhardt, *J. Phys. Chem. B*, 2007, **111**, 4440-4445.
- 3 R. Mitzner, J. Rehanek, J. Kern, S. Gul, J. Hattne, T. Taguchi, R. Alonso-Mori, R. Tran, C. Weniger, H. Schörder, W. Quevedo, H. Laksmono, R. G. Sierra, G. Y. Han, B. Lassalle-Kaiser, S. Koroidov, K. Kubicek, S. Schreck, K. Kunnus, M. Brzhezinskaya, A. Firsov, M. P. Minitti, J. J. Turner, S. Moeller, N. K. Sauter, M. J. Bogan, D. Nordlund, W. F. Schlotter, J. Messinger, A. Borovik, S. Techert, F. M. F. de Groot, A. Föhlisch, A. Erko, U. Bergmann, V. K. Yachandra, P. Wernet and J. Yano, *J. Phys. Chem. Lett.*, 2013, **4**, 3641-3647.
- 4 R. Golnak, J. Xiao, K. Atak, J. S. Stevens, A. Gainar, S. L. M. Schroeder and E. F. Aziz, *Phys. Chem. Chem. Phys.*, 2015, **17**, 29000-29006.
- 5 K. Atak, R. Golnak, J. Xiao, E. Suljoti, M. Pflüger, T. Brandenburg, B. Winter and E. F. Aziz, *J. Phys. Chem. B*, 2014, **118**, 9938-9943.
- 6 J. Xiao, R. Golnak, K. Atak, M. Pflüger, M. Pohl, E. Suljoti, B. Winter and E. F. Aziz, *J. Phys. Chem. B*, 2014, **118**, 9371-9377.
- 7 K. Atak, R. Golnak, J. Xiao, M. Pflüger, T. Brandenburg, B. Winter and E. F. Aziz, *Phys. Chem. Chem. Phys.*, 2015, **17**, 3409-3414.
- 8 R. Golnak, J. Xiao, K. Atak, M. Khan, E. Suljoti and E. F. Aziz, *J. Phys. Chem. B*, 2015, **119**, 3058-3062.
- 9 S. S. N. Lalithambika, R. Golnak, B. Winter and K. Atak, *Inorg. Chem.*, 2019, **58**, 4731-4740.
- 10 M. Fondell, S. Eckert, R. M. Jay, C. Weniger, W. Quevedo, J. Niskanen, B. Kennedy, F. Sorgenfrei, D. Schick, E. Giangrisostomi, R. Ovsyannikov, K. Adamczyk, N. Huse, P. Wernet, R. Mitzner and A. Föhlisch, *Struct. Dyn.*, 2017, **4**, 054902.
- 11 J. D. Koralek, J. B. Kim, P. Brůža, C. B. Curry, Z. Chen, H. A. Bechtel, A. A. Cordones, P. Sperling, S. Toleikis, J. F. Kern, S. P. Moeller, S. H. Glenzer and D. P. DePonte, *Nat. Commun.*, 2018, **9**, 1353.
- 12 R. M. Jay, S. Eckert, R. Mitzner, M. Fondell and A. Föhlisch, *Chem. Phys. Lett.*, 2020, **754**, 137681.
- 13 R. Büchner, M. Fondell, R. Haverkamp, A. Pietzsch, V. V. da Cruz and A. Föhlisch, *Phys. Chem. Chem. Phys.*, 2021, **23**, 24765-24772.
- 14 J. W. Smith and R. J. Saykally, *Chem. Rev.*, 2017, **117**, 13909-13934.
- 15 M. Nagasaka, H. Yuzawa and N. Kosugi, *Anal. Sci.*, 2020, **36**, 95-105.
- 16 M. Nagasaka and N. Kosugi, *Chem. Lett.*, 2021, **50**, 956-964.
- 17 H. Yuzawa, M. Nagasaka and N. Kosugi, *J. Phys. Chem. C*, 2015, **119**, 7738-7745.
- 18 M. Nagasaka, H. Yuzawa, T. Horigome, A. P. Hitchcock and N. Kosugi, *J. Phys. Chem. C*, 2013, **117**, 16343-16348.
- 19 F. Kumaki, M. Nagasaka, R. Fukaya, Y. Okano, S. Yamashita, S. Nozawa, S. Adachi and J. Adachi, *J. Chem. Phys.*, 2023, **158**, 104201.

- 20 M. Nagasaka, T. Hatsui, T. Horigome, Y. Hamamura and N. Kosugi, *J. Electron Spectrosc. Relat. Phenom.*, 2010, **177**, 130-134.
- 21 M. Nagasaka, H. Yuzawa, T. Horigome and N. Kosugi, *J. Electron Spectrosc. Relat. Phenom.*, 2018, **224**, 93-99.
- 22 M. Nagasaka, K. Mochizuki, V. Leloup and N. Kosugi, *J. Phys. Chem. B*, 2014, **118**, 4388-4396.
- 23 K. A. de Villiers, C. H. Kaschula, T. J. Egan and H. M. Marques, *J. Biol. Inorg. Chem.*, 2007, **12**, 101-117.
- 24 A. V. Luzanov, A. A. Sukhorukov and V. É. Umanskii, *Theor. Exp. Chem.*, 1976, **10**, 354-361.
- 25 R. L. Martin, *J. Chem. Phys.*, 2003, **118**, 4775-4777.
- 26 I. Mayer, *Chem. Phys. Lett.*, 2007, **437**, 284-286.
- 27 A. V. Luzanov and O. A. Zhikol, in *Practical Aspects of Computational Chemistry I*, ed. J. Leszczynski and M. K. Shukla, Springer, Heidelberg, Germany, 2011, pp. 415-449.
- 28 T. Yanai, D. P. Tew and N. C. Handy, *Chem. Phys. Lett.*, 2004, **393**, 51-57.
- 29 A. D. Spaeth, N. L. Gagnon, D. Dhar, G. M. Yee and W. B. Tolman, *J. Am. Chem. Soc.*, 2017, **139**, 4477-4485.
- 30 B. A. Hess, *Phys. Rev. A*, 1986, **33**, 3742-3748.
- 31 G. Jansen and B. A. Hess, *Phys. Rev. A*, 1989, **39**, 6016-6017.
- 32 T. Nakajima and K. Hirao, *Chem. Rev.*, 2012, **112**, 385-402.
- 33 H. Tatewaki, S. Yamamoto and Y. Hatano, *ACS Omega*, 2017, **2**, 6072-6080.
- 34 J. V. Jorstad, T. Xie and C. M. Morales, *Int. J. Quant. Chem.*, 2022, **122**, e26881.
- 35 B. Johansson and N. Mårtensson, *Phys. Rev. B*, 1980, **21**, 4427-4457.